Modeling and Analysis of New Processes for Polyester and Nylon Production

Zhen Yao and W. Harmon Ray
Dept. of Chemical Engineering, Univ. of Wisconsin, Madison, WI 53706

Integrated processes for nylon and polyester production were simulated. The polyester process includes four stages: esterification, prepolycondensation, finishing stage, and solid-state polycondensation. Three stages are involved in the nylon process: prepolycondensation, melt polycondensation, and the solid-state stage. The effect of beginning the solid-state stage at lower DP (compared to the value of the current process) was investigated for both nylon and polyester production. Reactors with either cocurrent or countercurrent purge gas flow were applied to the finishing stage for polyester and to the melt stage for nylon. The performance of different reactors was compared. The effect of purge gas strongly depended on the mass-transfer capacity of reactors. In the nylon process, variations in purge gas conditions had a small effect on reactor performance. However, purge gas effects on the polyester process were considerable, and countercurrent flow was more effective than cocurrent flow. The reactor operated at atmospheric pressure and, with countercurrent gas flow, can readily substitute for traditional high vacuum operation in the finishing stage of the polyester process.

Introduction

Polyesters and polyamides (nylons) are important commercial polycondensation polymers. In addition to their commanding positions as textile fibers, nylons can be readily processed through extrusion or injection molding to yield mechanical and electrical parts while polyesters are playing an important role in the automotive tire cord and beverage bottle markets. Recently, several new processes have been proposed for polyester and nylon production. In current solid-state polycondensation processes (Kaushik and Gupta, 1992; Kulkarni and Gupta, 1994; Papaspyrides, 1992; Srinivasan et al., 1994), polymer particles with moderate molecular weights are heated to a temperature between their glass transition and melting points and polymerized to high molecular weight. Recent patents and presentations (Leffew, 1999; Stouffer et al., 1996a,b,c, 1997, 1998) suggest how these processes can be operated with dramatically lower molecular weight feed materials in order to reduce the time required in the melt finishing step. Other patents (Bhatia, 1995, 1996) also suggest using inert purge gas in the finishing stage reactor. It has been reported that a finishing reactor operated at atmospheric pressure with purge gas flow can readily substitute for the current high vacuum finishing stage. In this work, these new processes are investigated for commodity products polyethylene terephthalate (PET) and nylon 6,6.

Correspondence concerning this article should be addressed to W. Harmon Ray.

PET Process

Chemistry and kinetics

PET is generally produced through two different routes with different raw materials: dimethyl terephthalate (DMT)-ethylene glycol (EG) and terephthalic acid (TPA)-ethylene glycol (EG). DMT was more commonly used when high purity TPA was very expensive and TPA solubility was a process issue. However, since fiber grade TPA is now a commodity and the solubility issue has been handled effectively, most PET plants in the world now use the TPA-EG route (Ravindranath and Mashelkar, 1986a,b).The reaction mechanisms for PET production are shown as follows (Ravindranath and Mashelkar, 1984). Kinetics constants presented by Ravindranath and Mashelkar (1984) are applied in this work (Table 1).

Table 1. Kinetic Constants for PET Production

Reaction	Activation Energy (kcal/mol)	Frequency Factor (kg/mol/h)	Equilibrium Constant
Esterification	17.6	1.52×10^{8}	1.25
Transesterification	18.5	9.91×10^{7}	0.5
Acetaldehyde formation	29.8	5.0×10^{7}	—
DEG formation	29.8	6.06×10^{9}	—
Vinyl endgroup formation	37.8	2.2×10^{7}	—
Reaction of vinyl endgroup	18.5	9.91×10^{7}	—

Reaction 1: Esterification

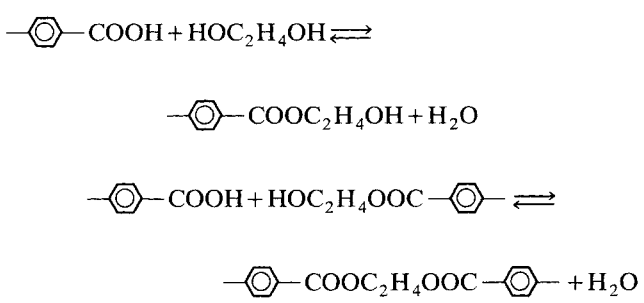

Reaction 2: Transesterification

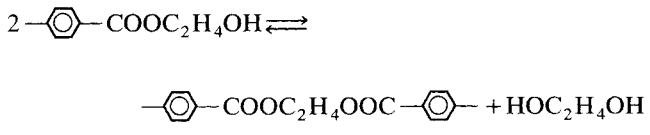

Reaction 3: Ultimate Monomer Degradation (Acetaldehyde Formation)

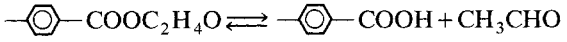

Reaction 4: Diethyleneglycol (DEG) Formation

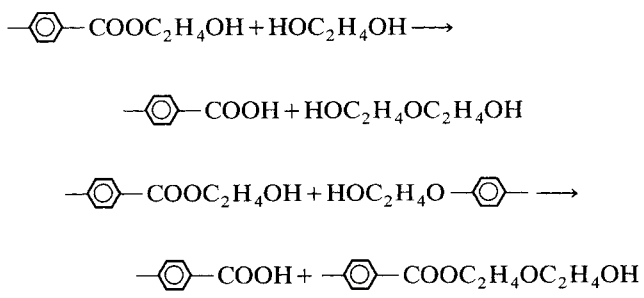

Reaction 5: Repeating Unit Degradation (Vinyl Formation)

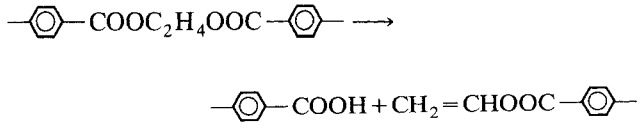

Reaction 6: Reaction of Vinyl End Group

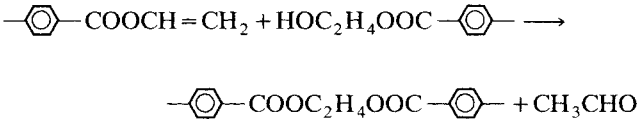

The starting material TPA/EG cannot be mixed readily because TPA is a crystalline solid that shows low solubility in EG. However, TPA solubility in bis(hydroxyethyl) tereph thalate (BHET) and other oligomers (produced in esterification reaction) is higher than in EG. Therefore, the overall solubility of TPA in the reaction mixture is increased during the esterification process.

The dependence of TPA solubility in EG on temperature has been determined by many researchers (Baranova and Kremer, 1977; Krumpolc and Malek, 1973; Yamada et al., 1985; Yang et al., 1996), and described as follows

$$\ln C = A - B/T$$

Here, C is the TPA concentration in mol/kg, T is temperature in K, and A, B are constants. In this study, the parameters from Baranova and Kremer's (1977) work are used. For EG, $A = 1.19$, $B = 1.24$, and, for BHET and oligomers, $A = 1.9$ and $B = 1.42$. It is assumed that the TPA dissolution rate is fast so that equilibrium solubility exists while solid TPA is present.

Conventional High Vacuum Process

Figure 1 shows the flowsheet of a current technology integrated process for the TPA-EG route. The process consists of four stages: esterification, pre-polycondensation, melt polycondensation, and solid-state polycondensation. Operat-

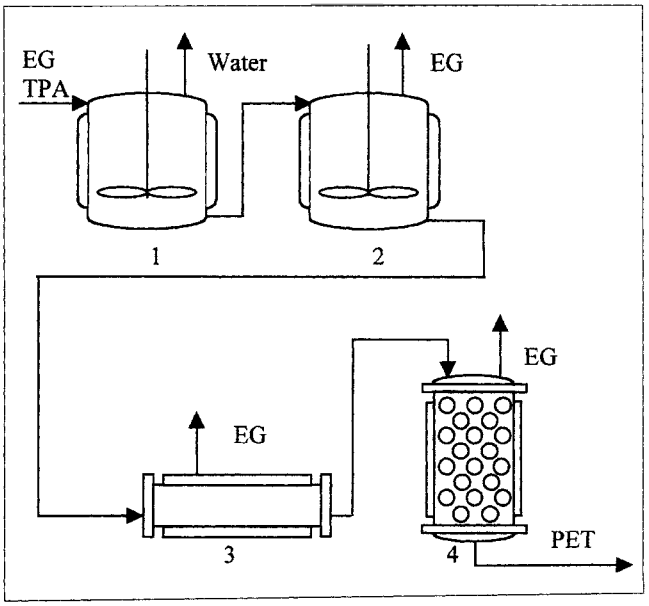

Figure 1. Flowsheet for PET production.

1 Esterification; 2 prepolycondensation; 3 finishing stage; 4 solid-state stage.

Table 2. PET: Operating Condition of Reactors

Variable	Temperature (°C)	Pressure (torr)	Residence Time (s)
Esterification	260	3,000	10,800
Prepolycondensation	270	50	7,800
Finishing stage	290	5	5,400
Solid-state stage	235	760	25,200

ing conditions of the different stages are listed in Table 2. It can be seen that the first reactor is carried out at 3,000 torr, pre-polycondensation and finishing reactors are operated at vacuum conditions, and the solid-state stage is at atmospheric pressure. As shown in Table 3, the EG content of feed flow is twice the TPA content on a mol basis.

The simulation of this process was carried out in the POLYRED package (UWPREL, 1999). POLYRED is a user-friendly package with a highly modular structure which aims to be a comprehensive simulation environment for polymerization process analysis and design. POLYRED CPC modules incorporate general modeling for polycondensation in various reactors, such as tank, tube, tower and particle/gas tank reactor (PTNK). Here, the CPC_TANK module is used for the esterification and pre-polycondensation stage, while CPC_TUBE and CPC_PTNK modules are used for the finishing reactor and solid-state stages, respectively. Table 4 presents a brief description and references to details of these modules.

As stated in this table, mass transfer between two phases can be simulated dynamically in all CPC modules. The mass-transfer rate is calculated through the following equation

$$\dot{N} = k_L S_V (a_m - a_v)$$

where k_L and S_V are the mass-transfer coefficient and mass-transfer area, while a_m and a_v are the activities in the melt phase and vapor phase respectively. The activity in the vapor phase can be calculated by assuming ideal gas behavior while the equilibrium activity in the melt phase is calculated using Flory-Huggins theory.

The dynamic evolution of the number average chain length DP for each stage of the process is shown in Figure 2. Although, in practice, there are some variations in the exit DP values from stage to stage, we consider here the following staging. In the first stage BHET is produced through the direct esterification reaction between TPA and EG, and this reacts further to oligomers. In the second stage, BHET and oligomers are polymerized to a DP of 12. Then, the product goes through a melt polycondensation reactor and further polymerized to a DP of about 80 under high vacuum conditions. Finally, the solid-state polycondensation stage is used to increase DP to 145.

Table 3. PET: Feed Conditions

Variable	Value
Feed rate (kg/s)	0.05
Condensate concentration (mol/kg)	0
EG concentration (mol/kg)	6.8966
TPA concentration (mol/kg)	3.4483

Table 4. POLYRED Modules Used for the Simulation

Modules	Simple Description	References
CPC_TANK	Models the dynamics of polycondensation in well-mixed tank reactors with two inlet and two outlet streams. Two phases are present in the tank: a melt phase, where reaction occurs, and a vapor phase, with mass transfer between the two phases.	Jacobsen and Ray, 1992a,b
CPC_TUBE	Models the dynamics of polycondensation in a tubular geometry. Two phases are present, a melt phase where reaction occurs, and a vapor phase, with mass transfer between the two phases.	Hipp and Ray, 1996
CPC_PTNK	Models the dynamics of polycondensation in a gas/particle system. The diffusion of volatile component inside particles and the mass transfer between two phases are modeled. The reactor can be specified as a stirred bed or a moving bed.	Mallon and Ray, 1998b,c

Figure 3 shows the change of TPA concentration with time at each stage. It can be seen that almost all of the TPA is consumed during the esterification and pre-polycondensation stages. There is little monomer present in the finishing and solid-state reactors. As shown in Figure 4, most of the dieth ylene glycol (DEG) is produced in the first two reactors so that DEG concentrations change very little in the third and fourth stages.

Expanded Solid-State Stage

The finishing stage for PET requires relatively long residence times, high vacuum operation, and mechanical power to generate the thin films and large surface area necessary to achieve high molecular weight in the highly viscous melt. By contrast, the solid-state stage is operated at atmospheric pressure, at lower temperature, and with little or no mechan-

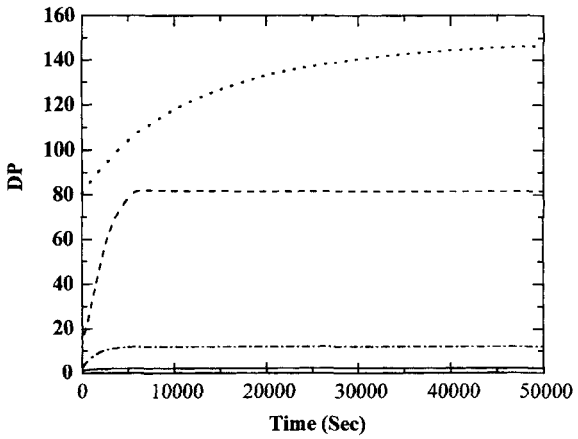

Figure 2. PET: time evolution of DP at the outlet of reactors.

—— Esterification reactor; ·—· prepolycondensation reactor; - melt polycondensation reactor; ... SSP reactor.

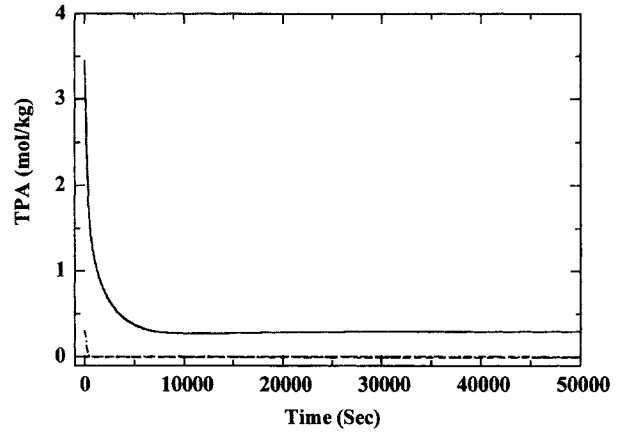

Figure 3. PET: time evolution of TPA at the outlet of reactors.

—— Esterification reactor; · — · prepolycondensation reactor; - melt polycondensation reactor; · · · SSP reactor.

ical agitation. Thus, it has been proposed (Leffew, 1999; Stouffer et al., 1996a,b,c, 1997, 1998) that higher production rates and lower process costs could be achieved by reducing the polymer DP and melt viscosity exiting the finishing stage, and then feeding particles of this lower DP to the solid-state reactors. In order to operate the solid-state stage at greatly reduced feed DP values, one must be able to create suitably crystalline particles with sufficiently high particle sticking temperature in order to avoid particle agglomeration. Recent work by Dupont (Leffew, 1999; Stouffer et al., 1996a,b,c, 1997, 1998) suggest these problems can be overcome.

Since the reaction temperature of the solid-state stage is generally lower than that in the finishing reactor, one can expect a longer residence time for the whole process. Table 5 shows how much residence time in the solid-state stage is needed to obtain a DP of 145 with different feed DP values. The overall residence time increases rapidly with the decrease in DP of polymers in the feeding stream. Although the residence time in the finishing reactor is reduced due to the

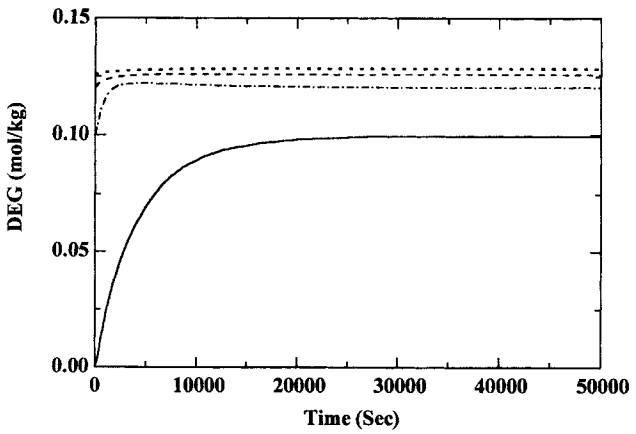

Figure 4. PET: time evolution of DEG at the outlet of reactors.

—— Esterification reactor; · — · prepolycondensation reactor; - melt polycondensation reactor; · · · SSP reactor.

Table 5. PET: Processes with Different DP Values in the Feedstream to the SSP Reactor

DP at inlet of SSP Reactor		80	60	40	25
Residence time in SSP reactor (s)	$d^* = 0.266$ cm	25,200	54,000	84,000	144,000
	$d^* = 0.14$ cm	11,000	21,000	36,000	57,600
Residence time in finishing reactor (s)		5,400	3,126	1,705	710
Overall capacity (kg/s)		0.05	0.087	0.158	0.380

*d is the diameter of the particles.

decrease in exit product molecular weight, the residence time in the downstream solid-state stage increases rapidly as feed DP is lowered.

There are several ways to reduce the residence time needed in solid-state stage. As shown in Table 5, a smaller particle size can lead to a dramatic decrease in residence time due to the shorter diffusion distance and larger particle surface area per unit volume. This effect is more significant for lower feed DP values since more condensate is produced at low DP values. An increase in purge gas-flow rate can lower the condensate concentration in the vapor phase and increase the mass-transfer rate. However, the effect is not very significant since the diffusion of condensate inside the particles is the controlling step. For example, in a process with feed DP of 25 and particle diameter of 0.14 cm, the DP outlet value increases only from 145 to 146.8 when the purge gas-flow rate is increased by a factor of 10.

Even though the expanded solid-state stage would increase the overall process residence time, the higher efficiency of the finishing reactor with lower DP product has compensating advantages. The viscosity of the PET melt drops from about 200 Pa-s to 30 Pa-s when the DP is reduced from 80 to 40 (Leffew, 1999). This sharp decrease in melt viscosity leads to less mechanical power consumption and easier temperature control. Additionally, the vacuum conditions in the finishing reactor can be much less severe for lower outlet DP values. For example, PET with a DP of 40 can be produced at 30 torr vacuum instead of the 5 torr vacuum required for a DP 80 product. As shown in Table 5, there is also a possibility to increase the overall capacity by just enlarging the solid-state stage capacity while keeping the finishing reactor unchanged. This strategy can be considered for scale-up since the finishing reactor is more complicated and expensive than the SSP reactor.

Process with purge gas finisher

In the conventional PET process discussed above, the finishing reactor is operated at vacuum as high as 5 torr to remove the condensate and other volatile byproducts. Such processes require expensive vacuum equipment and high costs of operation. In this section, less costly atmospheric pressure polyester processes are studied. These processes incorporate an inert purge gas that removes the volatile byproducts. As shown in Figure 5, the process can be one of two types according to the relative flow direction of inert purge gas and melt polymer flow: cocurrent flow or countercurrent flow.

Figure 6 shows the performance of the cocurrent process as compared to the conventional reactor without gas flow, but operated at high vacuum. It can be seen that the purge

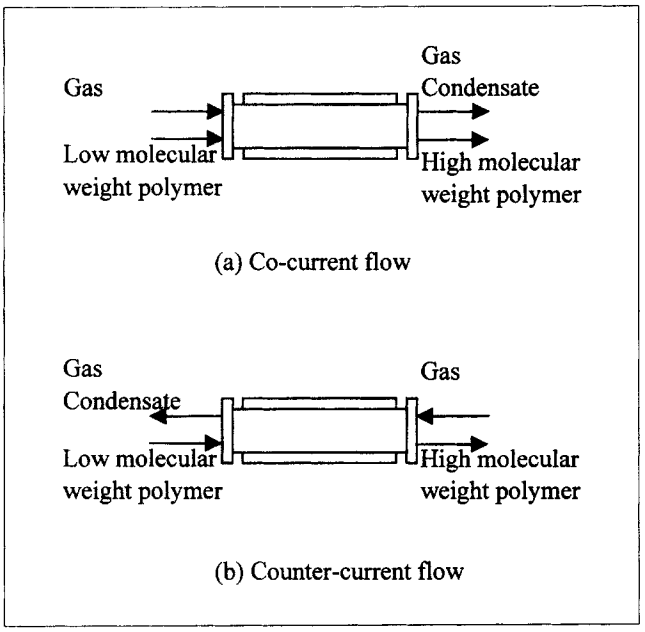

Figure 5. Reactors with purge gas flow.

gas-flow rate has a significant effect on final molecular weight, and high molecular weight polymer can be produced at atmospheric pressure with sufficiently high gas-flow rate. The profiles of DP, as well as melt phase and vapor-phase EG activity at steady state, are shown in Figure 7. Note that the vapor-phase EG activity in the cocurrent process increases along the reactor and reaches a maximum value at the outlet of reactor where the melt phase activity has its minimum value. In the vacuum case, the gas-flow rate is zero. At any given position inside the reactor, EG is evaporated from the melt phase into the gas phase at the same position. Since the EG concentration decreases along the reactor in the melt phase,

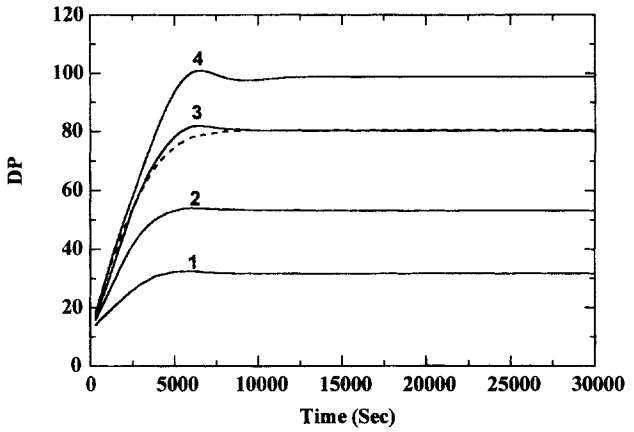

Figure 6. PET: time evolution of DP at the outlet of different finishing reactors.

Cocurrent flow: —— reactors operated at atmospheric pressure and with cocurrent gas flow, gas /polymer (kg/kg): (1) 0.25, (2) 1.0, (3) 3.5, (4) 10; --- reactor at 5 torr and without gas flow; mass-transfer capacity of all the reactors is 6.7×10^{-6} mol/s·torr·L.

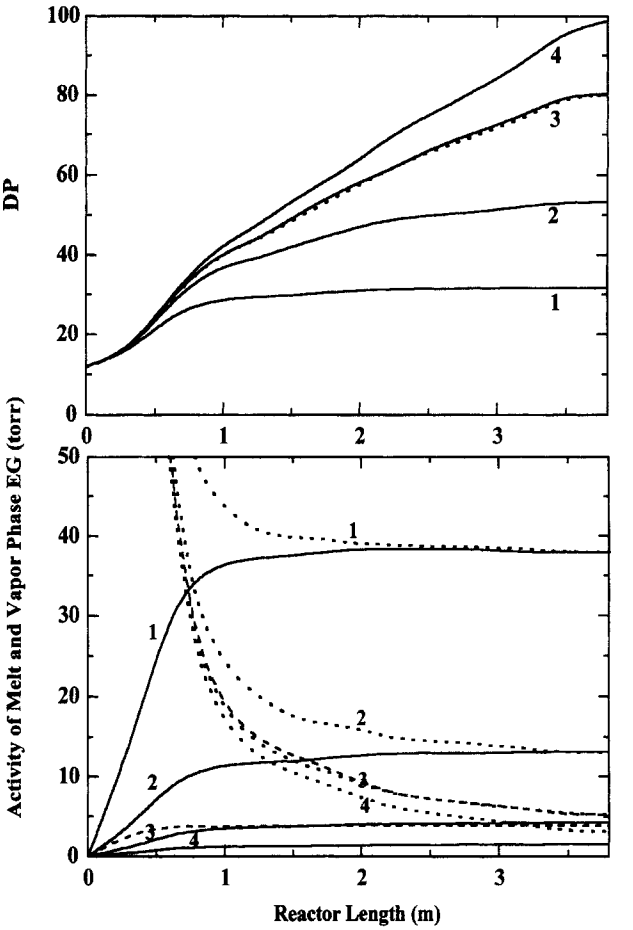

Figure 7. PET: profile of DP, melt-phase and vapor-phase EG activity inside different finishing reactors at steady state.

Reactors operated at atmospheric pressure and with cocurrent gas flow, gas/polymer (kg/kg): (1) 0.25, (2) 1.0, (3) 3.5, (4) 10, melt phase ..., vapor phase ——; reactor at 5 torr and without gas flow, --- ; mass-transfer capacity of all the reactors is 6.7×10^{-6} mol/s·torr·L.

nonuniform vaporization leads to a concentration profile in the gas phase.

Figures 8 and 9 show the performance of countercurrent flow operation that is significantly better than cocurrent flow operation. Note that the vapor-phase EG activity decreases along the reactor and reaches a minimum value at the point where the melt phase activity also has a minimum. Thus, as one might expect, compared with cocurrent operation, countercurrent operation has greater overall driving force for mass transfer, leading to improved finishing reactor performance.

The results, as summarized in Table 6, show that either operation could replace the conventional high vacuum finisher; however, countercurrent operation has significant advantages. For example, in order to get the same DP as with the high vacuum process, the ratio of gas to polymer in cocurrent flow purge gas operation should be 3.5, but it is only 0.25 in countercurrent flow, very close to the value 0.22 reported by Bhatia (1999). This very low purge gas operating cost makes the process economically feasible.

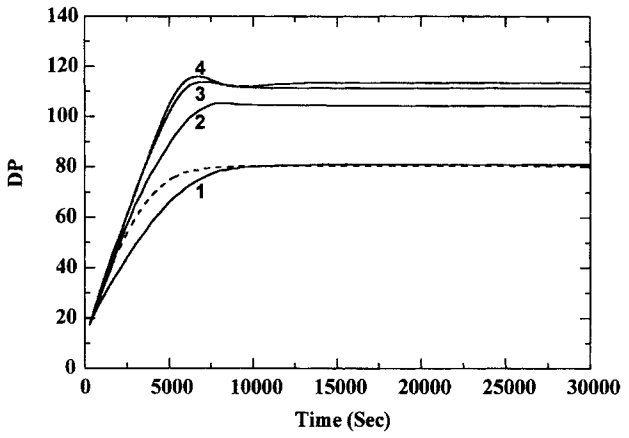

Figure 8. PET: time evolution of DP at the outlet of different melt reactors.

Countercurrent flow: —— reactors operated at atmospheric pressure and with countercurrent gas flow, gas/polymer (kg/kg): (1) 0.25, (2) 1.0, (3) 3.5, (4) 10; – – – reactor at 5 torr and without gas flow; mass-transfer capacity of all the reactors is 6.7×10^{-6} mol/s·torr·L.

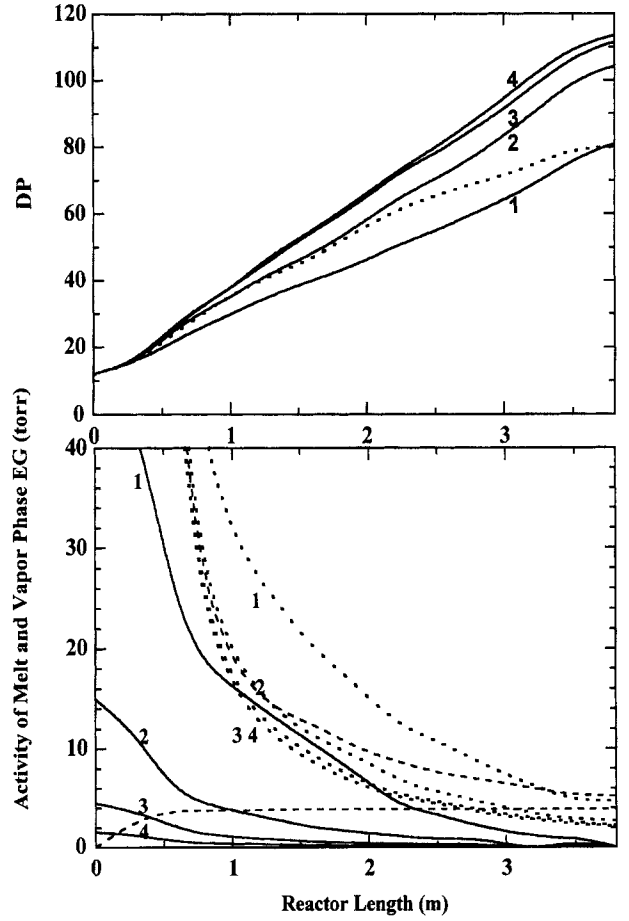

Figure 9. PET: profile of DP, melt-phase and vapor-phase EG activity inside different finishing reactors at steady state.

Reactors operated at atmospheric pressure and with countercurrent gas flow, gas/polymer (kg/kg): (1) 0.25, (2) 1.0, (3) 3.5, (4) 10, melt phase ···, vapor-phase ——; reactor at 5 torr and without gas flow, – – –; mass-transfer capacity of all the reactors is 6.7×10^{-6} mol/s·torr·L.

Table 6. PET: Cocurrent vs. Countercurrent Flow Processes

Gas/Polymer Mass Flow Rate*		DP at Outlet of Reactor	
		Cocurrent Flow	Countercurrent Flow
0	(5 torr)	80	
0.25	(760 torr)	31.65	81.00
1	(760 torr)	53.23	104.32
3.5	(760 torr)	80.39	111.43
10	(760 torr)	98.81	113.58

*All processes in this table have the same residence time (5,400 s) and temperature (290°C) in the melt phase.

All of the above discussions are based on a finishing reactor with a mass-transfer capacity of 6.7×10^{-6} mol/s·torr·L. The effect of mass-transfer capacity, which is defined as the product of mass-transfer coefficient and mass-transfer area, is presented in Tables 7 and 8. The disc ring contactor is widely used as a PET finishing reactor. How, very limited information is available for the mass-transfer coefficient of disc ring reactors. The following equation is presented by Ravetkar and Kale (1981) to correlate their experimental data

$$\frac{k_L d}{D} = 1.59\left(\frac{d^2 n}{D}\right)^{0.5}$$

Here, D is the diffusivity of the solute in the melt, and n is the rotational speed of the disc and ring. The diffusivity of EG in PET is on the order of 10^{-8} m^2/s (Pell and Davis, 1973) in the reaction temperature range. The mass coefficient varies from 6.05×10^{-6} to 1.44×10^{-4} mol/s-torr-m^2 as n varied from 1 ~ 30 rpm. As reported in DuPont patents (Bhatia, 1995, 1996, 1999), the mass-transfer area of a finish-

Table 7. Exit Value of DP for the PET Process with Cocurrent Purge Gas Flow: Effect of Mass-Transfer Capacity

Gas/Polymer Mass Flow Rate*		Mass Transfer Capacity, mol/s·torr·L			
		0.67×10^{-6}	3.0×10^{-6}	6.7×10^{-6}	24.0×10^{-6}
0	(5 torr)	26.64	57.55	80	92.79
0.25	(760 torr)	24.21	31.58	31.65	31.80
1.0	(760 torr)	26.25	47.47	53.23	53.92
3.5	(760 torr)	26.89	58.60	80.39	92.01
10	(760 torr)	27.07	63.06	98.81	135.38

*All processes in this table have the same residence time (5,400 s) and temperature (290°C) in the melt phase.

Table 8. Exit Value of DP for the PET Process with Countercurrent Purge Gas Flow: Effect of Mass Transfer Coefficient

Gas/Polymer Mass Flow Rate*		Mass Transfer Capacity, mol/s·torr·L			
		0.67×10^{-6}	3.0×10^{-6}	6.7×10^{-6}	24.0×10^{-6}
0	(5 torr)	26.64	57.55	80	92.79
0.25	(760 torr)	26.02	53.62	81.00	93.62
1.0	(760 torr)	26.85	62.04	104.32	129.97
3.5	(760 torr)	27.03	64.73	111.43	172.58
10	(760 torr)	27.13	65.50	113.58	194.52

*All processes in this table have the same residence time (5,400 s) and temperature (290°C) in the melt phase.

ing reactor is at least 0.067 m^2/L. Therefore, the mass-transfer capacity ranges from 4.05×10^{-7} to 9.67×10^{-6} mol/s·torr·L. One may notice that the mass-transfer capacity used in this work is much smaller the value reported by Cheong and Choi (1995). However, Cheong and Choi used a different mass-transfer driving force in their model. In this work the mass-transfer rate is calculated through the difference between the activities in melt phase and vapor phase, while Cheong and Choi based their mass-transfer rate on the difference between the bulk and interfacial EG concentration in the melt.

As shown in Tables 7 and 8, the effect of purge gas-flow rate on exit DP strongly depends on the mass-transfer capacity of the finisher. The effect on a reactor with adequate mass-transfer capacity is significant as indicated above. However, for very low mass-transfer capacity the effect can be small. For example, in a reactor with a very low mass-transfer capacity of 0.67×10^{-6} mol/s·torr·L, the exit DP only increased from 24 to 27 as the ratio of gas to polymer flow rates was raised from 0.25 to 3.5.

The profiles of DP, as well as melt-phase and vapor-phase activity for a low mass-transfer capacity of 0.67×10^{-6} mol/s·torr·L are plotted in Figures 10 and 11. This can be compared with Figures 7 and 9 for which the reactor has the much higher mass-transfer capacity of 6.7×10^{-6} mol/s·torr·L. It can be seen that the activity driving force in a reactor with low mass-transfer capacity is much larger than that in a reactor with high mass-transfer capacity. However, the small mass-transfer capacity is the dominating factor, which cannot be overcome by increasing purge gas-flow rates. Fortunately, values of mass-transfer capacity found in industrial finishers would seem to allow efficient atmospheric purge gas operation as a replacement for high vacuum operation.

Obviously, there is the need for optimizing the staging of exit DP, the design value of mass-transfer capacity, the purge gas rate, and so on in order to determine the most economical process. With such process optimization, using experimentally validated model parameters, the present modeling approach would be a valuable tool for process design and scale-up.

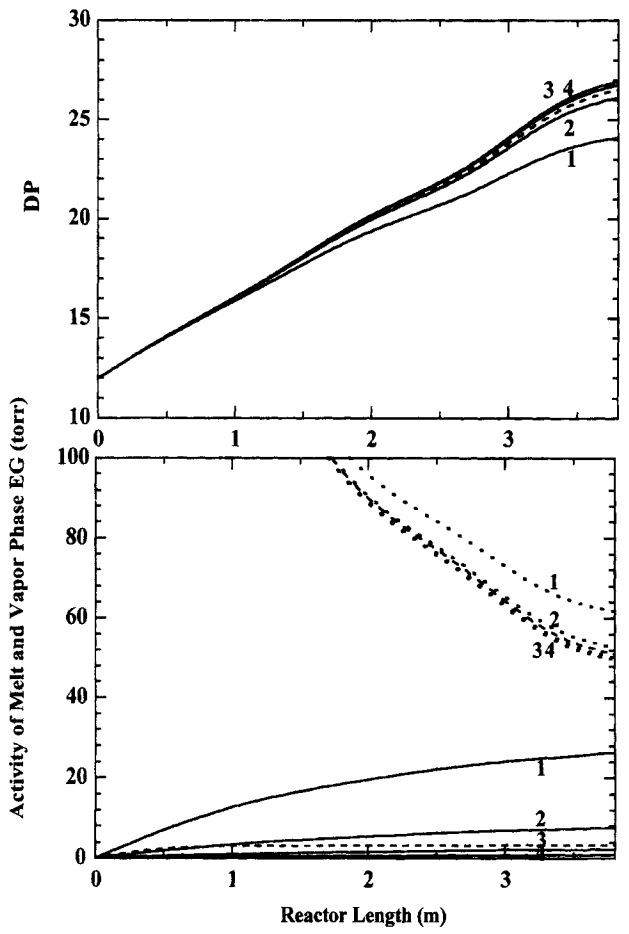

Figure 10. PET: profile of DP, melt-phase and vapor-phase EG activity inside different finishing reactors at steady state.

Reactors operated at atmospheric pressure and with co-current gas flow, gas/polymer (kg/kg): (1) 0.25, (2) 1.0, (3) 3.5, (4) 10, melt phase ···; vapor phase ——; reactor at 5 torr and without gas flow, – – – ; mass-transfer capacity of all the reactors is 0.67×10^{-6} mol/s·torr·L.

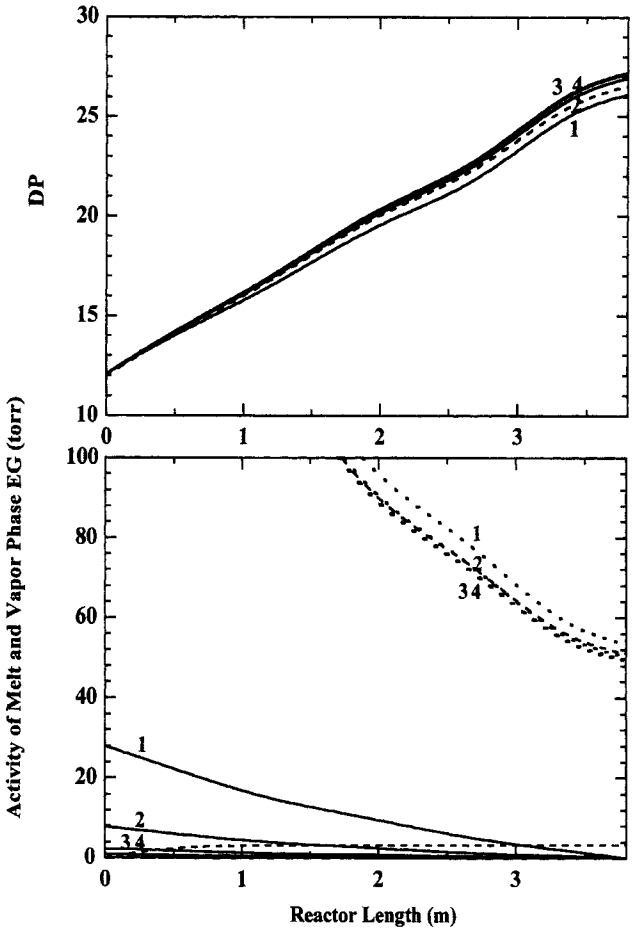

Figure 11. PET: the profile of DP, melt-phase and vapor-phase EG activity inside different finishing reactors at steady state.

Reactors operated at atmospheric pressure and with countercurrent gas flow, gas/polymer (kg/kg): (1) 0.25, (2) 1.0, (3) 3.5, (4) 10, melt phase ···; vapor phase ——; reactor at 5 torr and without gas flow, – – –; mass-transfer capacity of all the reactors is 0.67×10^{-6} mol/s·torr·L.

Table 9. Kinetic Parameters for Nylon 6,6 Production

Variable	Value
Ethalpy of polycondensation reaction	404.15 cal/mol
Entropy of polycondensation reaction	12.503 cal/mol/°C
Rate of polycondensation at 230°C	0.007065 $L^2/mol^2/h$
Activation energy for polycondensation	8,578 cal/mol
Dielectric kinetics parameter	40,716 cal/mol
Exponential term for dielectric constant	4,041 cal/mol
Preexponential factor for dielectric constant	0.06681

Nylon 6,6 Process

Chemistry and kinetics

Nylon 6,6 is produced from hexamethylene diamine (HMDA) and adipic acid (AA). The principal chain building reaction is as follows

$$-COOH + H_2N- \rightleftarrows -CONH- + H_2O$$

The apparent dependence of nylon equilibrium and kinetic constants on water concentration has been reported by many researchers. A number of empirical expressions and fundamental models were developed to describe the effect of water content (Giori and Hayes, 1970a,b; Mallon and Ray, 1998a; Ogata, 1961; Steppan et al., 1987; Wiloth, 1971; Tai et al., 1979; Tai and Tagawa, 1982). In this work, the fundamental model presented by Mallon and Ray (1998a) is used. This model is based on two states of water in the nylon melt: bound and free water. As shown below, the bound water is hydrogen bonded to the carbonyl group in nylon polymer chain; free water is simply unbound water

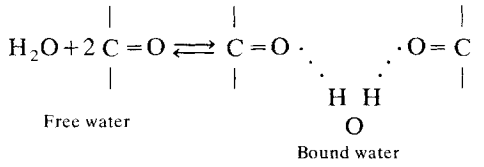

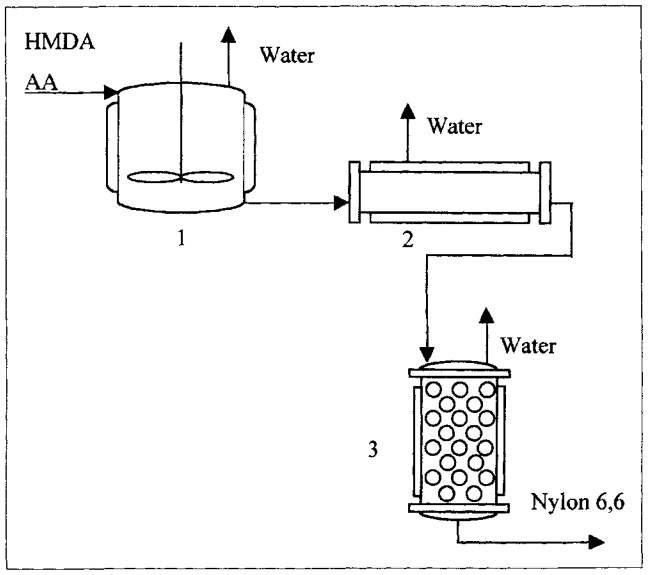

Figure 12. Flowsheet for nylon 6,6 production.

1 Prepolycondensation; 2 melt polycondensation; 3 solid-state stage.

Table 10. Nylon 6,6: Feed Conditions

Variable	Value
Feed rate (kg/s)	0.0278
Water concentration (mol/kg)	13.889
HMDA concentration (mol/kg)	2.8588
Adipic acid concentration (mol/kg)	2.8588

The following reaction mechanism was proposed to describe the role of water in nylon polymerization:

$$-COOH + H_2N- \rightleftarrows -COO^-\text{---}N^+H_3- \rightleftarrows -CONH- + H_2O$$

The first step is similar to the salting reaction, and the second reaction is the rate controlling step. The free water greatly affects the dielectric constant of the reaction mixture due to its high polarity. A higher dielectric constant makes the lefthand side of the "salting" reaction more stable, and reduces the amount of intermediate that is involved in the rate controlling step. Therefore, the apparent reaction rate is decreased with an increase in water concentration. Table 9 shows the kinetic parameters used in this model. More details are available in Mallon and Ray's work (1998a).

Conventional process

Figure 12 shows a typical flowsheet for nylon 6,6 production, which includes three stages: pre-polycondensation, melt polycondensation, and solid-state polycondensation. The feed and operating conditions of the different reactors are shown in Tables 10 and 11. A large amount of water can be found in the feedstream. The presence of water and higher pressure in the first stage can inhibit the vaporization of HMDA and dehydration of adipic acid. Further downstream, there is little HMDA and adipic acid; thus, the other two reactors are operated under atmospheric pressure. Here, it is assumed that HMDA recovery systems are used as necessary to prevent any significant HMDA loss.

The POLYRED package is also used for the simulation of this process. Figure 13 shows the dynamic evolution of DP at the outlet of the different stages. A low molecular weight polymer with DP of 12 is produced in the first reactor. The polymer is further polymerized to a DP of about 80 in the melt polycondensation reactor, and then passed onto a solid-state polycondensation reactor to achieve a high molecular weight with DP greater than 130. The HMDA and AA concentrations in different reactors are shown in Figure 14, where as expected, almost all of the monomer is consumed in the pre-polycondensation stage.

Because the equilibrium constant for nylon is hundreds of times larger than that for PET, much higher condensate con-

Table 11. Nylon 6,6: Operating Condition of Reactors

Variable	Prepoly-condensation	Melt Polycondensation	Solid-State Polycondensation
Temperature (°C)	254	267	202
Pressure (torr)	13,680	760	760
Residence time (s)	3,400	4,000	7,200

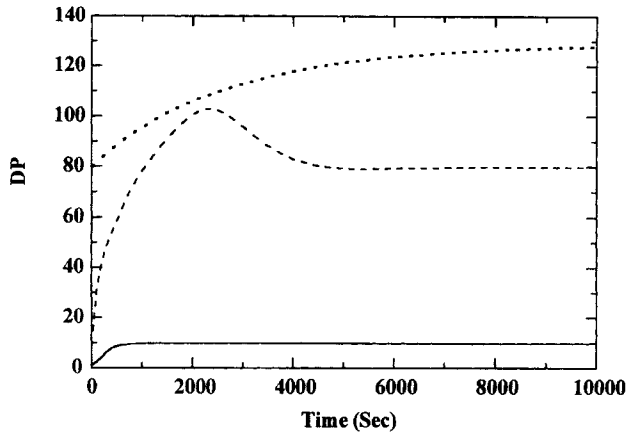

Figure 13. Nylon 6,6: time evolution of DP at the outlet of reactors.

—— Prepolycondensation reactor; – – – melt polycondensation reactor; · · · SSP reactor.

centration can be tolerated while achieving high molecular weight. Thus, for nylon, the condensate removal requirements are much less severe than for PET. This leads one to expect less dramatic improvements through expanded solid-state operation or purge gas finisher as compared to the PET process.

Expanded Solid-State Operation

Table 11 compares processes with different molecular weight at the outlet of the melt polycondensation reactors. As expected, the residence time in the melt stage decreases with decreasing exit DP values. However, the residence time in the solid-state reactor increases rapidly with a decrease of DP in the feed. Additionally, as shown in Table 12, the size of nylon particles does not have a considerable effect on the residence time needed in the solid-state stage. This can be explained by the large equilibrium constant for nylon polycondensation, which can tolerate much higher condensate concentrations in the particle without serious rate reduction. Therefore, for nylon 6,6, whether or not the expanded solid-state operation is better than the conventional process depends on the relative operating costs of the finishing and melt stages and the value of a capacity increase. However, cost improvements and the capacity increase are much less than that for the PET process.

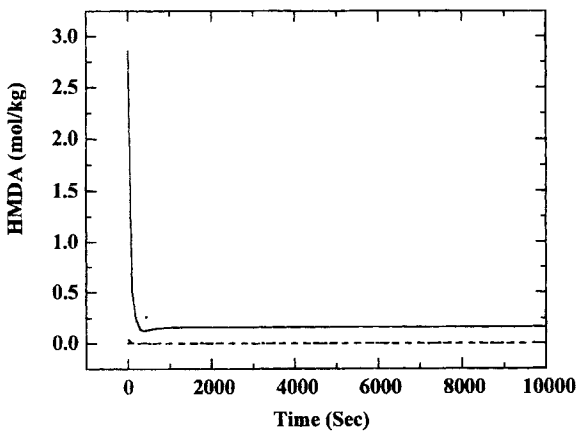

Figure 14. Nylon 6,6: time evolution of HMDA concentration at the outlet of reactors.

—— Prepolycondensation reactor; – – – melt polycondensation reactor; · · · SSP reactor.

Table 12. Nylon 6,6: Processes with Different DP Values in the Feedsteam to the SSP

DP at inlet of SSP Reactor		80	60	40	25
Residence time in SSP reactor (s)	d^* = 0.266 cm	7,200	12,000	20,000	30,000
	d^* = 0.14 cm	7,000	11,500	17,500	28,000
Residence time in finishing reactor (s)		4,000	3,200	2,133	1,066
Overall capacity (kg/s)		0.0278	0.0348	0.0520	0.1042

*d is the diameter of the particles.

Process with purge gas-flow finisher

For the nylon 6,6 process, the effects of purge gas flow on the melt stage are also investigated. Figure 15 shows the time evolution of DP at the outlet of the melt polycondensation reactor with cocurrent gas flow. The performance of the reactor without gas flow is described by the dashed line; while the solid lines denote reactors with cocurrent gas flow. The ratios of gas to polymer flow rate range from 0.007 to 7. As expected the use of purge gas can lead to higher polymer molecular weight, especially at high gas to polymer ratios. However, the effect is not very significant. The DP only increases from 80 to 90 as the gas/polymer ratio increases from 0 to 7. Figure 16 shows the profiles of DP, as well as the melt phase and gas-phase activity.

The performance of countercurrent flow process is shown in Figure 17. In this case, the purge gas flow also has an

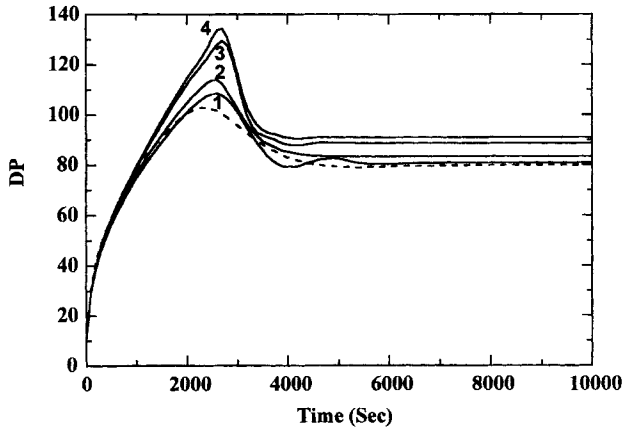

Figure 15. Nylon 6,6: time evolution of DP at the outlet of different melt reactors.

Cocurrent flow —— reactors operated at atmospheric pressure and with cocurrent gas-flow gas/polymer (kg/kg): (1) 0.007, (2) 0.07, (3) 0.7, (4) 7; – – – reactor at atmospheric pressure and without gas flow; mass-transfer capacity of all the reactors is 0.35×10^{-6} mol/s·torr·L.

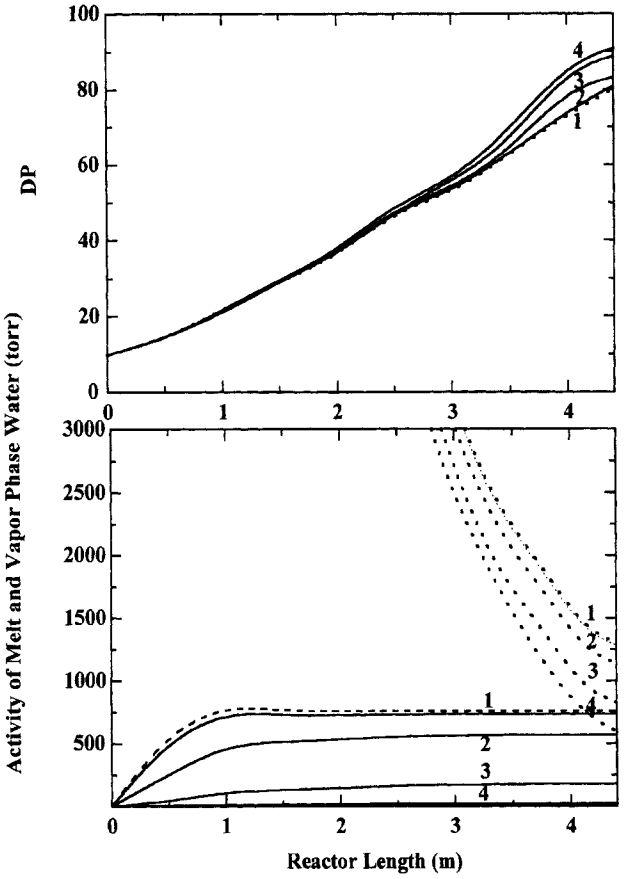

Figure 16. Nylon 6,6: profile of DP, melt-phase and vapor-phase water activity inside different melt reactors at steady state.

Reactors operated at atmospheric pressure and with cocurrent gas flow gas/polymer (kg/kg): (1) 0.007, (2) 0.07, (3) 0.7, (4) 7, melt-phase · · ·; vapor-phase ——; reactor at atmospheric pressure and without gas flow, – – –; mass-transfer capacity of all the reactors is 0.35×10^{-6} mol/s·torr·L.

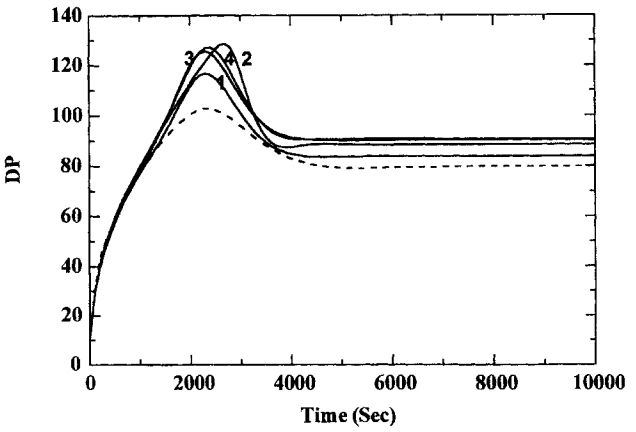

Figure 17. Nylon 6,6: time evolution of DP at the outlet of different melt reactors.

Countercurrent flow —— reactors operated at atmospheric pressure and with countercurrent gas-flow gas/polymer (kg/kg): (1) 0.007, (2) 0.07, (3) 0.7, (4) 7; – – – reactor at atmospheric pressure and without gas flow; mass-transfer capacity of all the reactors is 0.35×10^{-6} mol/s·torr·L.

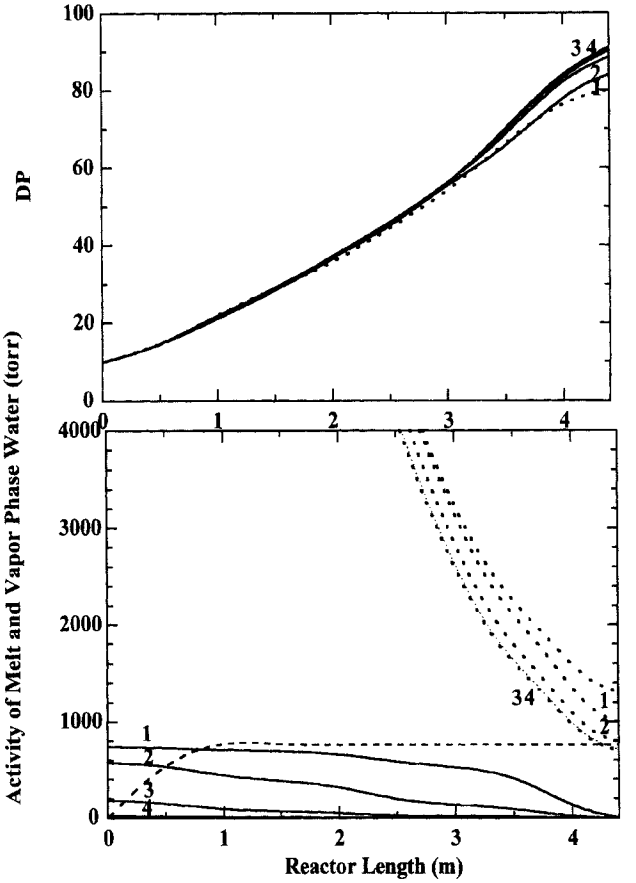

Figure 18. Nylon 6,6: profile of DP, melt-phase and vapor-phase water activity inside different melt reactors at steady state.

Reactors operated at atmospheric pressure and with countercurrent gas-flow gas/polymer (kg/kg): (1) 0.007, (2) 0.07, (3) 0.7, (4) 7, melt phase · · ·; vapor phase ——; reactor at atmospheric pressure and without gas flow, – – –; mass-transfer capacity of all the reactors is 0.35×10^{-6} mol/s·torr·L.

effect on nylon 6,6 production, but the results are not dramatic. The profiles of DP, as well as the melt-phase and vapor-phase water concentrations are shown in Figure 18.

Cocurrent and countercurrent flow processes are compared in Table 13. Although neither of the processes has a very large effect on the DP, the countercurrent flow process can produce higher DP product compared to the cocurrent flow process at the same gas to polymer ratio.

All of the above discussions are based on the melt polycondensation reactor with mass-transfer capacity of 0.35×10^{-6} mol/s·torr·L. Tables 14 and 15 show how the mass-transfer capacity of the reactor affects the results. It can be seen that the effects of purge gas flow become increasingly important as the mass-transfer capacity of the reactor is increased. The profiles of DP, as well as the melt-phase and vapor-phase water activity in the reactor with a mass-transfer capacity of 1.4×10^{-6} mol/s·torr·L are shown in Figures 19 and 20. In these figures, the activities of the two phases are very close to each other. An increase in gas-flow rate can lead to a considerable increase in the mass-transfer rate due to the large mass-transfer capacity of reactor. However, it is well known

Table 13. Nylon 6,6: Cocurrent vs. Countercurrent Flow Processes

Gas/Polymer Mass Flow Rate*	DP at Outlet of Reactor	
	Cocurrent Flow	Countercurrent Flow
0	80	
0.007	80.86	83.94
0.07	83.28	88.46
0.7	88.75	90.31
7	90.74	90.94

*All processes in this table have the same residence time (4,000 s) and temperature (266.5°C) in the melt phase.

that the equilibrium constant of nylon 6,6 polycondensation is very large. This means that high molecular weight polymer is possible even with significant water concentration in the melt phase. Thus, a reactor with large mass-transfer capacity is not essential in the nylon 6,6 process. Usually, in the commercial process, the mass-transfer capacity of reactor is on the order of 10^{-7} mol/s·torr·L (Jacobsen and Ray, 1992a). As shown above, the effect of purge gas flow is not very significant in this case.

Summary

Integrated processes for PET and nylon 6,6 production are simulated by using the POLYRED package. It has been found that high molecular weight nylon 6,6 and PET can be produced through processes involving solid-state polycondensation. The expanded solid-state stage requires longer residence times. However, this can be compensated for by the lower cost and higher capacity of the reduced viscosity finishing reactor, especially for PET production. The use of purge gas flow in the finishing reactor has a significant effect on

Table 14. Nylon 6,6 Process with Cocurrent Purge Gas Flow: Effect of Mass-Transfer Capacity

Gas/Polymer Mass Flow Rate*	Mass Transfer Capacity, mol/s·torr·L			
	0.35×10^{-6}	0.70×10^{-6}	1.40×10^{-6}	2.80×10^{-6}
0	80	109.88	121.95	126.88
0.007	80.86	110.51	122.64	127.83
0.07	83.28	114.92	128.46	134.30
0.7	88.75	127.13	145.38	154.04
7	90.74	132.73	153.56	166.58

*All processes in this table have the same residence time (4,000 s) and temperature (266.5°C) in the melt phase.

Table 15. Nylon 6,6 Process with Countercurrent Purge Gas Flow: Effect of Mass-Transfer Capacity

Gas/Polymer Mass Flow Rate*	Mass Transfer Capacity, mol/s·torr·L			
	0.35×10^{-6}	0.70×10^{-6}	1.40×10^{-6}	2.80×10^{-6}
0	80	109.88	121.95	126.88
0.007	83.94	124.71	148.11	164.73
0.07	88.46	131.42	149.97	157.86
0.7	90.31	133.02	153.38	166.19
7	90.94	133.51	154.67	166.37

*All processes in this table have the same residence time (4,000 s) and temperature (266.5°C) in the melt phase.

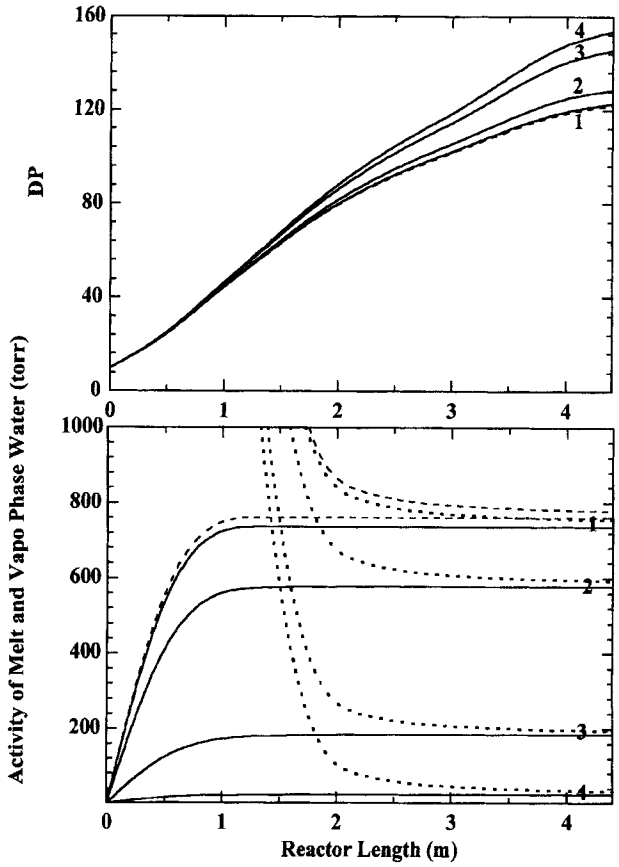

Figure 19. Nylon 6,6: profile of DP, melt-phase and vapor-phase water inside different melt reactors at steady state.

Reactors operated at atmospheric pressure and with cocurrent gas-flow gas/polymer (kg/kg): (1) 0.007, (2) 0.07, (3) 0.7, (4) 7, melt phase · · ·; vapor phase ——; reactor at atmospheric pressure and without gas flow; mass-transfer capacity of all the reactors is 1.40×10^{-6} mol/s·torr·L.

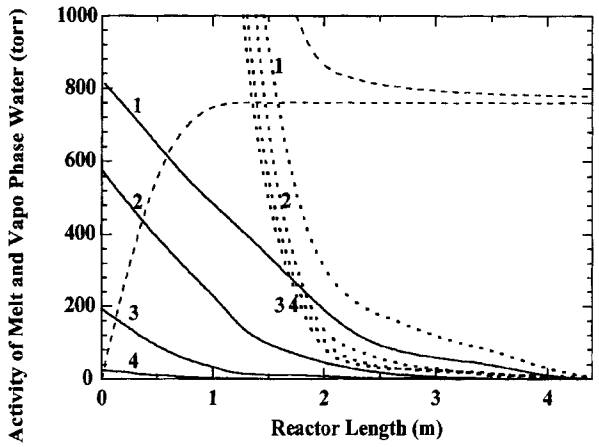

Figure 20. Nylon 6,6: profile of DP, melt-phase and vapor-phase water inside different melt reactors at steady state.

Reactors operated at atmospheric pressure and with countercurrent gas-flow gas/polymer (kg/kg): (1) 0.007, (2) 0.07, (3) 0.7, (4) 7, melt phase · · ·; vapor phase ——; reactor at atmospheric pressure and without gas flow, – – –; mass-transfer capacity of all the reactors is 1.40×10^{-6} mol/s·torr·L.

PET production, where countercurrent flow is more effective than cocurrent flow. It has been shown that a reactor operated at atmospheric pressure and with small countercurrent purge gas flow rates can readily match or exceed conventional high vacuum reactor performance. The use of purge gas operation for nylon 6,6 production does not yield large improvements unless the mass-transfer capacity is increased to that normally used for PET production.

Acknowledgments

The authors appreciate the financial support of the National Science Foundation and the industrial sponsors of the University of Wisconsin Polymerization Reaction Engineering Laboratory. We are grateful to Dr. George Kalfas for helpful comments and to Dr. Kamlesh Bhatia for valuable discussions during the review process.

Notation

a_m = melt-phase activity, torr
a_v = vapor-phase activity, torr
D = diffusivity of the solute, m^2/s
k_L = mass-transfer coefficient, $mol/s \cdot torr \cdot m^2$
n = rotational speed of the disc and ring
$\dot{N}$ = mass-transfer rate, $mol/L \cdot s$
S_V = mass-transfer area, m^2/L

Literature Cited

Baranova, T. L., and E. B. Kremer, "Solubility and Esterification Kinetics of Terephthalic Acid in Ethylene Glycol," *Khim. Volokna*, **19**, 16 (1977).

Bhatia, K. K., "Continuous Polyester Process," U.S. Patent to Du Pont, No. 5434239 (1995).

Bhatia, K. K., "Atmospheric Pressure Polyester Process," U.S. Patent to Du Pont, No. 5552513 (1996).

Bhatia, K. K., "Apparatus and Process for a Polycondensation Reaction," U.S. Patent to Du Pont, No. 5856423 (1999).

Cheong, S. I., and K. Y. Choi, "Melt Polycondensation of Poly(Ethylene Terephthalate) in a Rotating Disk Reactor," *J. Appl. Poly. Sci.*, **58**, 1473 (1995).

Giori, C., and B. T. Hayes, "Hydrolylic Polymerization of Caprolactam: 1. Hydrolysis—Polycondensation Kinetics," *J. Poly. Sci., Poly. Chem. Ed.*, **8**, 335 (1970a).

Giori, C., and B. T. Hayes, "Hydrolylic Polymerization of Caprolactam: 2. Vapor-Liquid Equilibria," *J. Poly. Sci., Poly. Chem. Ed.*, **8**, 351 (1970b).

Hipp, A. K., and W. H. Ray, "A Dynamic Model for Condensation Polymerization in Tubular Reactor," *Chem. Eng. Sci.*, **51**, 281 (1996).

Jacobsen, L. L., and W. H. Ray, "Analysis and Design of Melt and Solution Polycondensation Processes," *AIChE J.*, **38**, 911 (1992a).

Jacobsen, L. L., and W. H. Ray, "Unified Modeling for Polycondensation Kinetics," *J. Macromol. Sci.*, **C32**, 407 (1992b).

Kaushik, A., and S. K. Gupta, "A Molecular Model for Solid-State Polymerization of Nylon," *J. Appl. Poly. Sci.*, **45**, 507 (1992).

Krumpolc, M., and J. Malek, "Esterification of Benzenecarboxylic Acid with Ethylene Glycol,4—Kinetics of the Initial Stage of Polyesterification of Terephthalic Acid with Ethylene Glycol Catalyzed by Zinc Oxide," *Makromol. Chemie*, **171**, 69 (1973).

Kulkarni, A. R., and S. K. Gupta, "Molecular Model for Solid-State Polymerization of Nylon 6: 2. An Improved Model," *J. Appl. Poly. Sci.*, **53**, 85 (1994).

Leffew, K. W., "Advances in Condensation Polymerization," AIChE Meeting (1999).

Mallon, F. K., and W. H. Ray, "A Comprehensive Model for Nylon Melt Equilibrium and Kinetics," *J. Appl. Poly. Sci.*, **69**, 1213 (1998a).

Mallon, F. K., and W. H. Ray, "Modeling of Solid-State Polycondensation. 1. Particle Models," *J. Appl. Poly. Sci.*, **69**, 1233 (1998b).

Mallon, F. K., and W. H. Ray, "Modeling of Solid-State Polycondensation. 2. Reactor Design Issues," *J. Appl. Poly. Sci.*, **69**, 1775 (1998c).

Ogata, N., "Studies on Polycondensation Reaction of Nylon Salt: 2. The Rate of Polycondensation Reaction of Nylon 6,6 Salt in Water Solution," *Makromol. Chem.*, **43**, 117 (1961).

Papaspyrides, C. D., "Solid State Polyamidation Processes," *Polymer Inter.*, **29**, 293 (1992)

Pell, J. T. M., and T. G. Davis, "Diffusion and Reaction in Polyester Melts," *J. Poly. Sci.: Poly. Phys. Ed.*, **11**, 1671 (1973).

Ravetkar, D. D., and D. D. Kale, "Gas Absorption into Non-Newtonian Fluid in Rotating Disc Contactor," *Chem. Eng. Sci.*, **36**, 399 (1981).

Ravindranath, K., and R. A. Mashelkar, "Finishing Stages of PET Synthesis; a Comprehensive Model," *AIChE J.*, **30**, 415 (1984).

Ravindranath, K., and R. A. Mashelkar, "Chemistry, Thermodynamics and Transport Properties," *Chem. Eng. Sci.*, **41**, 2197 (1986a).

Ravindranath, K., and R. A. Mashelkar, "Polyethylene Tereph thalate: 2. Engineering Analysis," *Chem. Eng. Sci.*, **41**, 2969 (1986b).

Srinivasan, R., P. Desai, A. S. Abhiraman, and R. S. Knorr, "Solid State Polymerization Vis-à-Vis Fiber Formation of Step-Growth Polymer: 1. Result from a Study for Nylon 6,6," *J. Appl. Poly. Sci.*, **53**, 1731 (1994).

Steppan, D. D., M. F. Doherty, and M. F. Malone, "A Kinetics and Equilibrium Model for Nylon 6,6 Polymerization," *J. Appl. Poly. Sci.*, **33**, 2333 (1987).

Stouffer, J. M., E. N. Blanchard, and K. W. Leffew, "Production of Poly(Ethylene Terephthalate)," Patent to Du Pont, No. 5510454 (1996a).

Stouffer, J. M., E. N. Blanchard, and K. W. Leffew, "Production of Poly(Ethylene Terephthalate)," Patent to Du Pont, No. 5532333 (1996b).

Stouffer, J. M., E. N. Blanchard, and K. W. Leffew, "Process for Pellet Formation from Amorphous Polyester," Patent to Du Pont, No. 5540868 (1996c).

Stouffer, J. M., E. N. Blanchard, and K. W. Leffew, "Apparatus for Forming Crystalline Polymer Pellets," Patent to Du Pont, No. 5633018 (1997).

Stouffer, J. M., E. N. Blanchard, and K. W. Leffew, "Production of Poly(Ethylene Terephthalate)," Patent to Du Pont, No. 5714262 (1998).

Tai, K., and T. Tagawa, "The Kinetics of Hydrolytic Polymerization of Caprolactam: 5. Equilibrium Data on Cyclic," *J. Appl. Poly. Sci.*, **27**, 2791 (1982).

Tai, K., H. Teranishi, Y. Arai, and T. Tagawa, "The Kinetics of Hydrolytic Polymerization of Caprolactam," *J. Appl. Poly. Sci.*, **24**, 211 (1979).

UWPREL, "POLYRED V5.0 User's Manual," Madison, WI (1999).

Wiloth, F., "The Mechanism and Kinetics of Caprolactam Polymerization in the Presence of Water," *Makromol. Chem.*, **144**, 329 (1971).

Yamada, T., Y. Imamura, and O. Makimura, "A Mathematical Model for Computer Simulation of a Direct Continuous Esterification Process between Terephthalic Acid and Ethylene Glycol: 1. Model Development," *Poly. Eng. and Sci.*, **25**, 788 (1985).

Yang, K. S., K. H. An, C. N. Choi, S. R. Jin, and C. Y. Kim, "Solubility and Esterification Kinetics of Trephthalic Acid in Ethylene Glycol: 3. The Effect of Functional Group," *J. Appl. Poly. Sci.*, **60**, 1033 (1996).

Manuscript received Jan. 6, 2000, and revision received Aug. 1, 2000.